

ARF6 as a Novel Activator of HIF-2 α in Pulmonary Arterial Hypertension

Adam L. Fellows^{1*}, Chien-Nien Chen¹, Chongyang Xie¹, Nayana Iyer¹, Lukas Schmidt³, Xiaoke Yin¹, Luke A. Yates^{2,4}, Manuel Mayr¹, Andrew Cowburn¹, Lan Zhao¹, and Beata Wojciak-Stothard¹

¹National Heart and Lung Institute and ²Department of Infectious Disease, Imperial College London, London, United Kingdom; ³King's British Heart Foundation Centre, King's College London, London, United Kingdom; and ⁴Francis Crick Institute, London, United Kingdom

ORCID IDs: 0000-0002-9975-3795 (A.L.F.); 0000-0003-1177-5568 (L.Z.); 0000-0002-6607-7372 (B.W.-S.).

Abstract

ARF6 (ADP-ribosylation factor 6), a GTPase associated with cancer metastasis, is activated in the lung endothelium in pulmonary arterial hypertension (PAH). To identify ARF6-regulated pathways relevant to PAH, we performed a state-of-the-art proteomic analysis of human pulmonary artery endothelial cells (HPAECs) overexpressing the wild-type, constitutively active, fast-cycling, and dominant-negative mutants of ARF6. The analysis revealed a novel link of ARF6 with HIF (hypoxia-inducible factor), in addition to endocytotic vesicle trafficking, cell proliferation, angiogenesis, oxidative stress, and lipid metabolism. Active ARF6 markedly increased expression and activity of HIF-2, critical in PAH, with HIF-1 relatively unaffected. Hypoxic ARF6 activation was a prerequisite for HIF-2 activation and HIF-dependent gene expression in HPAECs, PAH blood-derived late-outgrowth endothelial colony-forming cells,

and hypoxic mouse lungs *in vivo*. A novel ARF6 inhibitor, chlortetracycline (CTC), reduced hypoxia-induced HIF-2 activation, proliferation, and angiogenesis in HPAECs and reduced HIF-2 expression in lung and heart tissues of hypoxic mice. PAH endothelial colony-forming cells showed elevated expression and activity of ARF6 and HIF2, which was attenuated by CTC, and oral CTC attenuated development of pulmonary hypertension in chronically hypoxic mice. We identify EGFR (epidermal growth factor receptor) as a direct interactor of ARF6 and EGFR signaling as a crucial mechanism linking ARF6 and HIF activation. In conclusion, we are the first to demonstrate a key role of ARF6 in the regulation of HIF-2 α activation *in vitro* and *in vivo* and show that HIF-2 α , a master regulator of vascular remodeling in PAH, can be targeted by a clinically approved antibiotic CTC.

Keywords: pulmonary arterial hypertension; hypoxia; endothelium

Pulmonary arterial hypertension (PAH) is a rare disease characterized by gradual narrowing of small and medium pulmonary arteries, ultimately leading to right heart failure and premature death (1). Pulmonary endothelial dysfunction, manifested by increased proliferation, resistance to

apoptosis, angiogenesis, and endothelial-to-mesenchymal transition, largely driven by HIF-2 (hypoxia-inducible factor-2), plays a critical role in initiation and progression of PAH (2, 3). ARF6 (ADP-ribosylation factor 6) has been implicated in pulmonary vascular remodeling in PAH (4), but

signaling mechanisms involved are not fully understood. ARF6 is a member of the ARF family of six proteins (ARF1–6), belonging to the Ras superfamily of small GTPases (5). Like other ARFs, ARF6 oscillates between an “active” GTP-bound state and an “inactive” GDP-bound state, with GTP binding and

(Received in original form March 28, 2024; accepted in final form November 18, 2024)

*Present address: Department of Comparative Biomedical Sciences, Royal Veterinary College, London, United Kingdom.

Supported by British Heart Foundation project grant PG/19/19/34286 and BHF Imperial Centre of Research Excellence grant RE/18/4/34215.

Author Contributions: Conceptualization and funding acquisition: B.W.-S. Data curation: A.L.F., C.-N.C., C.X., N.I., L.S., X.Y., L.A.Y., A.C., and B.W.-S. Formal analysis: A.L.F., C.-N.C., and L.A.Y. Investigation, project administration, supervision, validation, visualization, and writing – original draft: A.L.F. and B.W.-S. Methodology: A.L.F., C.-N.C., X.Y., M.M., A.C., L.Z., and B.W.-S. Resources: A.L.F., L.A.Y., M.M., A.C., L.Z., and B.W.-S. Writing – review & editing: A.L.F., C.-N.C., C.X., N.I., L.S., X.Y., L.A.Y., M.M., A.C., L.Z., and B.W.-S.

Correspondence and requests for reprints should be addressed to Beata Wojciak-Stothard, Ph.D., National Heart and Lung Institute, ICTEM Building, Hammersmith Campus, Imperial College London, Du Cane Road, London W12 0NN, UK. E-mail: b.wojciak-stothard@imperial.ac.uk.

This article has a related editorial.

This article has a data supplement, which is accessible at the Supplements tab.

Am J Respir Cell Mol Biol Vol 72, Iss 4, pp 380–392, April 2025

Copyright © 2025 by the American Thoracic Society

Originally Published in Press as DOI: 10.1165/rcmb.2024-0149OC on November 18, 2024

Internet address: www.atsjournals.org

Clinical Relevance

This project demonstrates the translational potential of a novel drug for treating pulmonary hypertension. We show that chlortetracycline, a clinically available antibiotic, has the ability to inhibit certain pathophysiological processes related to the response to low oxygen and attenuate pulmonary hypertension in an animal model.

hydrolysis mediated by GEFs (guanine nucleotide exchange factors) and GAPs (GTPase-activating proteins), respectively. Although the GTP-bound, membrane-associated form carries out most of the activities attributed to ARF6, its GDP-bound form together with regulatory proteins may also initiate signaling events (6). ARF6 is primarily known as a regulator of membrane receptor trafficking, vesicle transport, actin remodeling, and cell motility in various cell types, including metastatic cancer cells (7). Recent studies suggest that ARF6 may act as a modulator of hypoxic signaling in certain cell types (8), but specific mechanisms have not been delineated. PAH has a complex and multifaceted pathophysiology, including perturbed endothelial function and a heightened response to hypoxia. In this study, we aimed to identify key processes affected by ARF6 in human pulmonary endothelial cells, relevant to PAH. We report a novel pathway whereby ARF6 mediates the activation of HIF-2 α (hypoxia-inducible factor 2 α) in response to low oxygen tension both *in vitro* and *in vivo* and demonstrate effectiveness of a new ARF6 inhibitor, the antibiotic chlortetracycline (CTC), in the inhibition of HIF-2 signaling in healthy and PAH endothelial cells and a chronic hypoxia mouse model of pulmonary hypertension.

Some of the results of these studies have been previously reported in the form of a preprint (bioRxiv, 15 Sep 2023, <https://doi.org/10.1101/2023.09.15.557917>).

Methods

Detailed information can be found in data supplement.

Cell Culture

Human pulmonary artery endothelial cells (HPAECs) from different donors were purchased from Promocell (C-12241) and Lonza (CC-2530) and were cultured as previously described (9).

Adenoviral Gene Transfer

HPAECs were infected with recombinant adenoviruses to overexpress hemagglutinin-tagged ARF6 mutants: wild-type (WT-ARF6), constitutively active ARF6Q67L (CA-ARF6), fast-cycling ARF6T157A (FC-ARF6), and dominant-negative ARF6T27N (DN-ARF6). Empty adenoviruses (Vector Biolabs; 1.0×10^{12} pfu/ml) were used as adenoviral controls (AdCs). Adenoviral infection was carried out as previously described (4). Experiments were performed 24 hours after infection. ARF6 overexpression was confirmed by Western blotting, quantitative PCR, and immunocytochemistry.

Proteomics

HPAECs overexpressing AdC, WT, CA, FC, and DN ARF6 for 24 hours were lysed in Radioimmunoprecipitation assay buffer (EMD Millipore; 20-188) containing protease inhibitors. Sample preparation and data analysis procedures (10, 11) are described in the data supplement. The relative quantities of the molecules were normalized to the control (AdC) of the corresponding biological replicate to calculate the fold-change and then scaled using \log_2 transformation to perform statistical testing. To generate volcano plots, \log_2 fold-changes for each protein were analyzed by an unpaired Student's *t* test and then adjusted for multiple comparisons using the original FDR method of Benjamini and Hochberg, with a *q* value of 5%. These *q* values were plotted against \log_2 fold-change, with thresholds of *q* < 0.05 and fold-change ± 0.2 indicated by dotted lines. Proteins that met both of these thresholds were deemed differentially expressed.

Bioinformatics

Bioinformatics was performed using the functional enrichment analysis web tool WebGestalt (www.webgestalt.org). The basic parameters were as follows: Organism of Interest: *Homo Sapiens*; Method of Interest: GSEA (Gene Set Enrichment Analysis); Functional Database: GeneOntology (GO, Biological Process), Pathway (KEGG, Panther, Reactome, WikiPathway), Network (Kinase Site), Disease (DisGenet, GLAD4U,

OMIM), Drug (DrugBank, GLAD4U), Phenotype (Human Phenotype Ontology), Community-Contributed (Hallmark50). Results are presented in bubble plots as normalized enrichment score, false discovery rate (FDR) (*q* value), and count (number of proteins). All upregulated pathways identified by six bioinformatics databases (GO Biological Process, Hallmark, KEGG, Panther, Reactome, WikiPathway) induced by CA-ARF6 were integrated into an Enrichment Map using Cytoscape software (12, 13). The Enrichment Map and AutoAnnotate applications were used to create a summary network (excluding unclustered nodes) color-coded by heat map according to the neighborhood connectivity of the pathway clusters.

Late Outgrowth Endothelial Colony-Forming Cells

Endothelial colony forming cells were derived from peripheral blood samples and characterized, as previously described (4, 9, 14). All endothelial colony-forming cells (ECFCs) were used between passages 3 and 6. Demographic and clinical features of healthy subjects and patients with PAH are provided in the data supplement.

Statistical Analysis and Data Presentation

All graphs were analyzed and plotted using GraphPad Prism software (GraphPad Software Inc.). Statistical comparisons between three or more groups were performed with ordinary one-way or two-way ANOVA and Dunnett's multiple comparisons test. Statistical comparisons between two groups were performed using unpaired Student's *t* test. Gaussian distributions and equal SDs between groups were confirmed before statistical tests. Violin plots were used to present data with appropriate *P* values.

Results

Expression and Intracellular Localization of ARF6 Activity Mutants in HPAECs

To better understand the effects of ARF6, HPAECs were infected with recombinant adenoviruses to overexpress the WT-ARF6, CA-ARF6 (15, 16), FC-ARF6 (17), and DN-ARF6 (15, 16) (Figure 1A). In CA-ARF6, the GTP binding is resistant to hydrolysis; hence, the mutant remains permanently locked into an active,

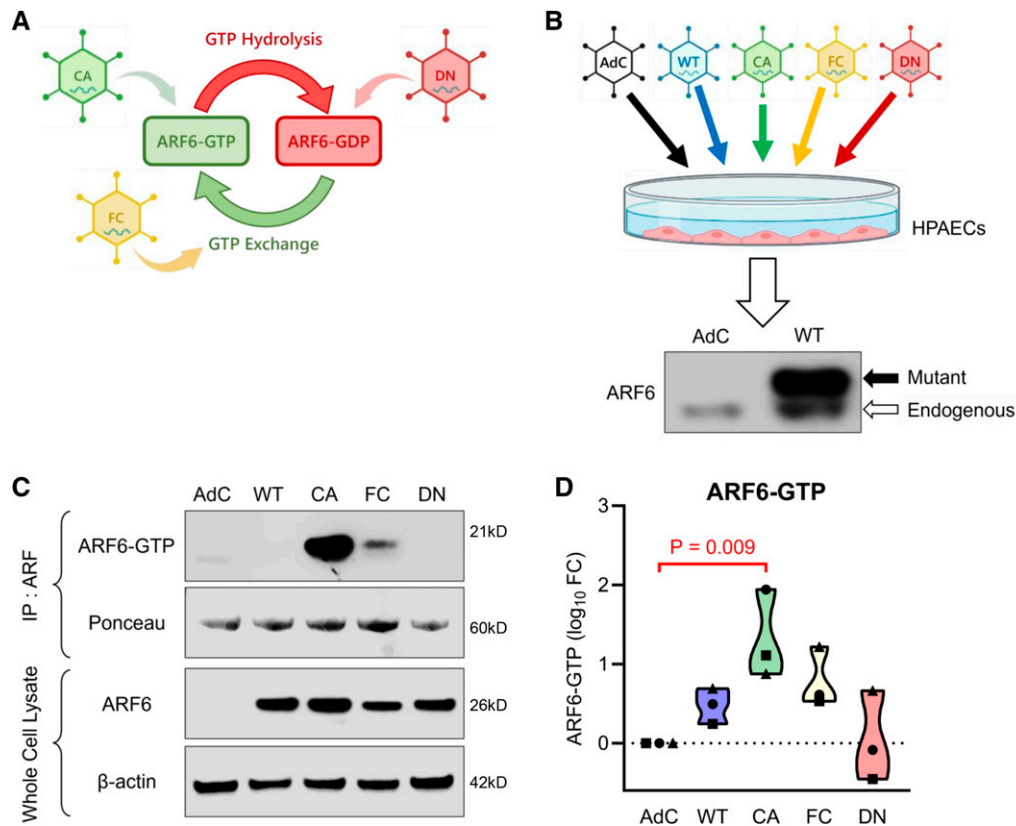


Figure 1. Adenoviral overexpression of ARF6 (ADP-ribosylation factor 6) activity mutants in human pulmonary artery endothelial cells (HPAECs). (A) Schematic illustrating effect of ARF6 mutations on GTP hydrolysis and GDP exchange. (B) Expression of endogenous and hemagglutinin-tagged mutant ARF6 (WT, CA, FC, and DN) was studied by Western blotting in HPAECs 24 hours post-transduction. Note: the immunoblot image for ARF6 is enlarged from that shown in Figure 2A for AdC and WT in Donor 4. (C) Representative Western blots and (D) a corresponding graph showing changes in the expression of active (GTP-bound) ARF6, total ARF6, and β -actin, as indicated. (D) Fold-changes normalized to the empty AdC ($n=3$ different biological replicates). P values obtained from one-way ANOVA with Dunnett's multiple comparisons test. AdC = adenoviral control; CA = constitutively active; DN = dominant negative; FC = fast cycling; IP = immunoprecipitation; WT = wild-type.

GTP-bound conformation. The FC-ARF6 mutant exhibits spontaneously higher rates of GTP exchange, while retaining a capacity for GTP hydrolysis, whereas the DN-ARF6 mutant displays defective GTP binding and is locked into an inactive, GDP-bound state (Figure 1B). Mutant proteins were effectively overexpressed in the vast majority of infected cells (see Figure E1 in the data supplement). To enable a comparative analysis, CA-ARF6 overexpression levels were adjusted to induce an ~ 10 -fold increase in ARF6 activity, corresponding to changes seen in PAH endothelial cells (4), and expression of other ARF6 mutants was equalized to that of CA-ARF6 (Figures 1C and 1D). Cell fractionation showed that CA-ARF6 localized predominantly to the cell membrane, whereas DN mutant, as predicted, showed mainly cytoplasmic localization (Figure E2). WT-ARF6 and FC-ARF6 mutants showed equal distribution

between the cell membrane and cytoplasm and were largely absent from cytoskeletal or nuclear fractions (Figure E2). ARF6 activity (GTP binding) was highest in CA-ARF6-overexpressing HPAECs, whereas FC-ARF6 had a more modest effect (Figures 1C and 1D).

Proteomic Analysis of HPAECs Overexpressing ARF6 Activity Mutants

An unbiased proteomic analysis was used to identify key processes affected by ARF6 activity changes in HPAECs. Robust and equal overexpression of ARF6 protein 24 hours after adenoviral transduction was confirmed by Western blotting in four different HPAEC donors (Figures 2A and 2B), and whole-cell lysates were subjected to a state-of-the-art proteomics workflow (Figure 2C), including tandem mass tag peptide labeling combined with liquid

chromatography with tandem mass spectrometry to ensure high-precision coverage and quantitation (18). The number of differentially expressed proteins varied among the ARF6 mutants, with WT-ARF6, CA-ARF6, FC-ARF6, and DN-ARF6 mutants generating 3, 14, 19, and 43 differentially expressed proteins, respectively (Figures 2D and E3). Enrichment analysis on ranked lists of all identified proteins against a range of curated databases (GO, Hallmark, KEGG, Panther, Reactome, WikiPathways) revealed that CA-ARF6 induced the highest number of pathway changes (559 upregulated, 282 downregulated) compared with WT-ARF6 (54 upregulated, 238 downregulated), FC-ARF6 (46 upregulated, 300 downregulated), or DN-ARF6 (117 upregulated, 292 downregulated) (Figure 2E). CA-ARF6 specifically enriched pathways associated with hypoxic signaling, including HIF, growth factors (EGF, FGF, VEGF),

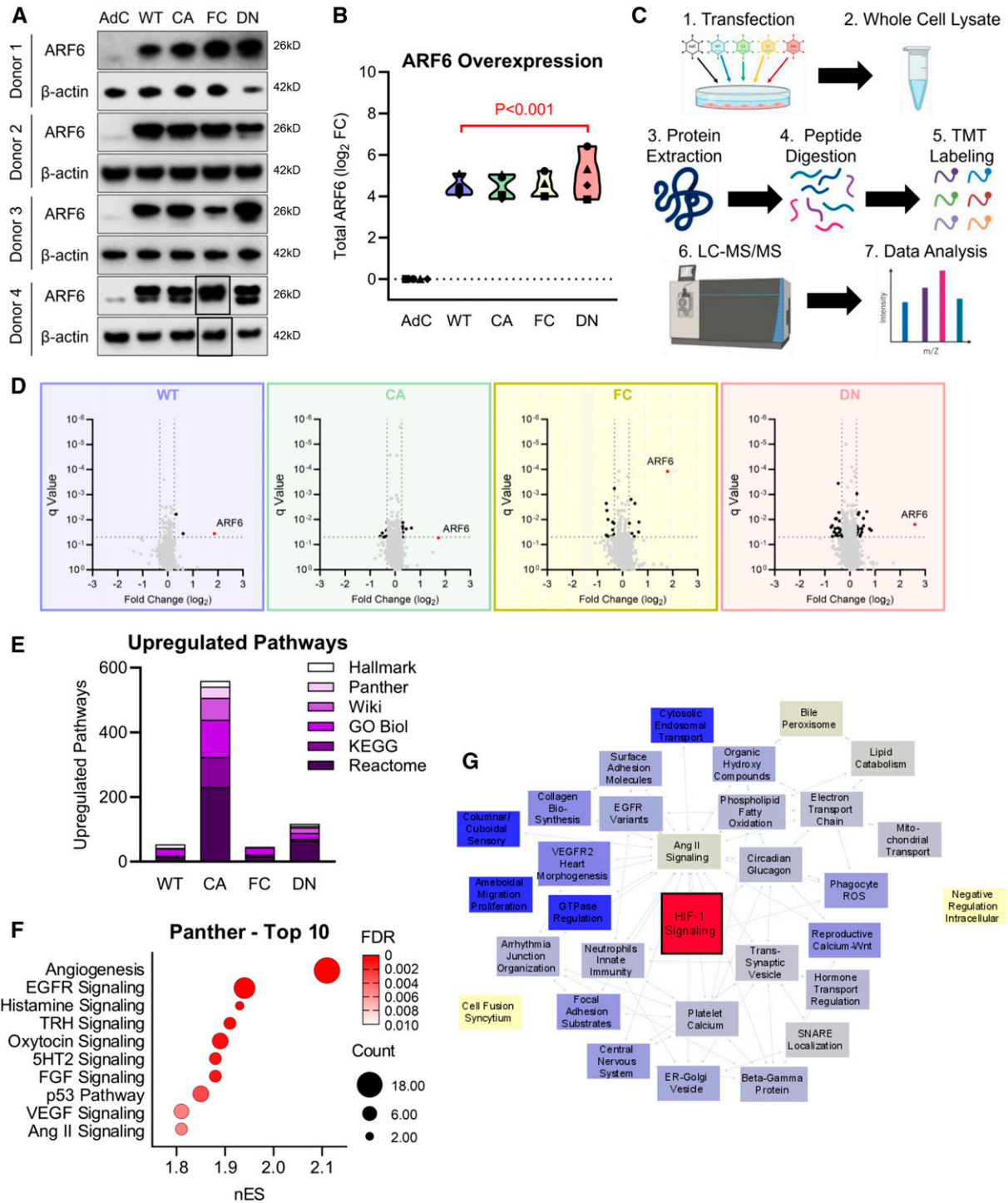


Figure 2. Proteomic analysis of HPAECs overexpressing ARF6 activity mutants. (A) Western blots and (B) quantification of total ARF6 overexpression in HPAECs from four different donors. *P* values obtained from one-way ANOVA with Dunnett's multiple comparisons test ($n=4$). (C) Proteomics workflow for HPAEC whole-cell lysates using TMT labeling followed by LC-MS/MS. (D) Volcano plots displaying the protein changes according to proteomic analysis for the four different ARF6 mutants; black symbols indicate differentially expressed proteins, with ARF6 highlighted in red. (E) Stacked bar chart showing the number of upregulated pathways induced by each ARF6 mutant, according to each bioinformatics database. (F) Bubble plot of the 10 most significantly upregulated Panther pathways by overexpression of CA-ARF6, with HIF (hypoxia-inducible factor) signaling highlighted in red. 5HT2 = serotonin receptor type 2; Ang II = angiotensin II; EGFR = epidermal growth factor receptor; GO Biol = GeneOntology Biological Process; FGF = fibroblast growth factor; KEGG = Kyoto Encyclopedia of Genes and Genomes; LC-MS/MS = liquid chromatography with tandem mass spectrometry; ROS = reactive oxygen species; TMT = tandem mass tag; TRH = thyrotropin-releasing hormone; VEGF = vascular endothelial growth factor.

vasoconstrictors (histamine, serotonin, ET-1, Ang II), and regulators of angiogenesis and glycolysis (Figure 2F and Table E8). An enrichment map integrating data from all the bioinformatics databases further highlighted the regulatory role of ARF6 in HIF signaling, in addition to its well-documented role in the vesicle transport (7) (Figure 2G). Using multiple databases was crucial, given that different pathway databases generate disparate results in statistical enrichment analyses (19).

ARF6 Induces Normoxic Activation of HIF

HIF transcription factors are master regulators of gene expression in PAH, with HIF-2 believed to play a causative role in the disease (20–22). HIF-2 activation by CA-ARF6 was confirmed by its nuclear translocation (\log_2 fold-change, 2.19 ± 1.10 , comparison with controls), whereas HIF-1 remained relatively unaffected (Figures 3A–3C). HIF activation was also confirmed by increased expression of luciferase reporter (\log_2 fold-change, 0.52 ± 0.17 change, comparison with controls) (Figure 3D) and increased expression of HIF-regulated genes, including *NOX4* (\log_2 fold-change, 0.88 ± 0.36), *RAB33A* (\log_2 fold-change, 1.01 ± 0.51), and *SLC2A1* (\log_2 fold-change, 0.50 ± 0.30) (Figure 3E).

Effect of ARF6 Activity on Endothelial Barrier Function and Proliferation *In Vitro*

CA-ARF6 enhanced expression of important structural components of endothelial adherens and tight junctions, including CDH5 (VE-Cadherin), PECAM-1 (CD31), and JAM3, as well as adhesion receptors for leukocyte recruitment, ICAM1, and ICAM2 (Figure 3F). CA-ARF6 significantly upregulated junctional signaling pathways and altered endothelial barrier function (Figures 3G and 3J), whereas other mutants had no effect. Increased expression of VE-cadherin was accompanied by its enhanced internalization (Figure 4), consistent with the documented role of ARF6 in the regulation membrane trafficking of this protein (23). CA-ARF6 increased expression of numerous cell proliferation markers, including *MAP2K2* (MEK2), *MAPK3* (ERK1), *PLCG1* (PLC γ 1), and *TEK* (TIE2) (Figure 3H), which resulted in enrichment of proliferation-related pathways (Figure 3I) and a time-dependent enhancement of HPAEC proliferation,

particularly evident after a prolonged time of overexpression (72 h) (Figure 3K). Cell apoptosis was not affected by ARF6 mutants (Figure E5). CA-ARF6 overexpression did not significantly alter expression or activity of the closely related ARF1 or other ARF family proteins (Figure E6). In summary, we show that sustained activation of ARF6 triggers normoxic activation of HIF-2 α and, to a lesser extent, HIF-1 and that this effect is accompanied by endothelial junctional remodeling and increased endothelial cell proliferation.

ARF6 Regulates Hypoxia-induced HIF Activation in HPAECs

Hypoxia is a key contributor to vascular remodeling in PAH (24). HPAECs exposed to hypoxia (1% O₂) showed a time-dependent increase in ARF6 activity, which peaked at 16 hours and remained elevated between 16 and 24 hours of hypoxic exposure, whereas ARF6 protein expression remained relatively unaffected (Figures 4A and E7A). The temporal activation profile of ARF6 peaked after 16 hours of hypoxia, which mirrored the time course of HIF-2 α accumulation in HPAECs (Figures 4A and 4B). HIF1- α activation in HPAECs, reported to reach maximum within 2–6 hours of the onset of hypoxia (25), did not correspond with changes in ARF6 activity. To further verify the role of ARF6 in the regulation of HIF activity, we tested the effects of the newly identified, ARF6-specific inhibitor chlortetracycline (CTC) (26). CTC reduced protein expression of HIF-2 α in a concentration-dependent manner, reduced expression of certain HIF-1 α and HIF-2 α target genes in hypoxic HPAECs (Figures 4C and 4D), inhibited hypoxia-induced endothelial cell proliferation, and prevented increased angiogenesis (Figures 4E–4G). The mRNA expression of HIF-1 α and HIF-2 α were unaffected by CTC (Figure E7B), suggesting that regulation of HIF by ARF6 likely occurs via post-translational modification. The specific inhibition of ARF6 by CTC is shown by no change in the activity of ARF1 (Figure E8). These findings demonstrate for the first time that ARF6 acts as a regulator of HIF-dependent endothelial responses to hypoxia *in vitro*.

ARF6 Regulates HIF Signaling at the Onset of Hypoxia *In Vivo*

To further verify our results and to test the role of ARF6 in the regulation of hypoxia-induced HIF signaling *in vivo*, mice were

exposed to acute hypoxia (10% O₂; 24 h), with one group receiving CTC (i.p., 77.3 mg/kg), before hypoxic exposure (Figure 5A). Hypoxia induced a significant increase in ARF6 activity in mouse lung tissues, which was reduced to normoxic expression levels by CTC (Figure 5B). Accumulation of HIF-2 α in hypoxia was reduced by CTC treatment (Figure 5B), and changes in HIF-2 α activity positively correlated with changes in ARF6 activity (Figure 5C). CTC markedly attenuated expression of HIF-2 α targets in the lung (Figure 5D) and reduced HIF-2 α expression in hypoxic lung and heart but not in kidney (Figures E9A and E9C), suggesting that its actions are tissue specific. Lung expression of HIF-1 α was undetectable, but even though heart and kidney showed higher expression of HIF-1 α , this was not affected by CTC (Figures E9B and E9D). Analysis of open-source data from the Human Protein Atlas, which is based on transcriptomic and antibody-based imaging, revealed that *Arf6* is expressed in various cell types in the human lung, with the highest expression levels noted in endothelial, alveolar epithelial, and immune cells (Figure E9F). Our results suggest a key role of ARF6 as an upstream regulator of HIF-2 and show that CTC, a novel and clinically available ARF6 inhibitor, reduces hypoxia-induced HIF signaling *in vivo*.

ARF6 Inhibition Attenuates Development of Chronic Hypoxia Pulmonary Hypertension in Mice

HIF signaling plays a key role in the initiation and development of chronic hypoxia-induced pulmonary hypertension, and here we studied the effects of CTC, administered in drinking water (40 mg/kg/d) to mice exposed to 14 days of hypoxia (10% O₂) (Figure 5E). CTC significantly reduced right ventricular hypertrophy (Figure 5F) and right ventricular systolic pressure (Figure 5G) and significantly reduced muscularization of small intrapulmonary arteries (Figures 5H and 5I). ARF6 activity was unchanged at 14 days of hypoxia (Figure E9G), suggesting that the protective effect of CTC on the development of chronic pulmonary hypertension is mediated by inhibition of ARF6 at the onset of hypoxia.

ARF6 Signaling in PAH

To gain further insight into the role in PAH, we identified ARF6 targets in publicly available PAH proteomic and transcriptomic PAH databases from PAH lung (4),

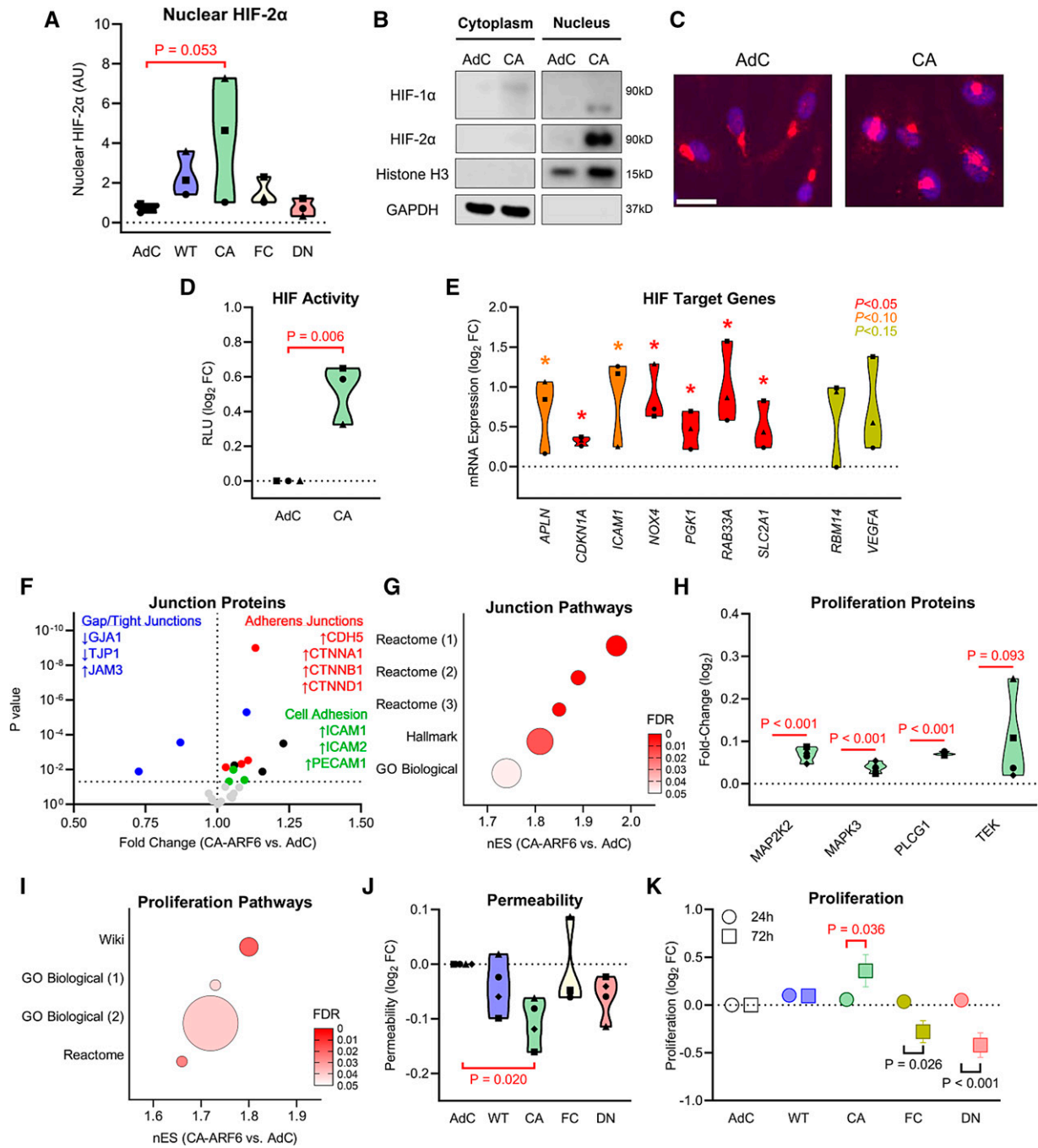


Figure 3. Active ARF6 induces HIF activity, alters junctions, and increases proliferation in HPAECs. (A) Quantification of HIF-2α in nuclear fractions of HPAECs overexpressing ARF6 mutants, as indicated; Western blotting ($n = 3$). (B) Representative Western blots showing cytoplasmic and nuclear localization of HIF-1α and HIF-2α. (C) Cellular distribution of HIF-2α (red) merged with nuclear stain (DAPI, blue), immunofluorescence; scale bars, 20 μm. (D) HIF activity measured by luciferase reporter assay in U2OS-HRE-Luc cells ($n = 3$ independent experiments). (E) Expression of selected HIF target genes by qRT-PCR ($n = 3$). (F) Volcano plot of selected junctional proteins from proteomic analysis of CA-ARF6. (G) Bubble plot showing enrichment of pathways referencing “Junctions” from different bioinformatics databases by CA-ARF6. (H) Violin plot of selected proliferation marker proteins from proteomic analysis of CA-ARF6. (I) Bubble plot showing enrichment of pathways referencing “Proliferation” from different bioinformatics databases by CA-ARF6. (J) FITC-dextran permeability assay ($n = 4$). (K) CyQUANT cell proliferation assay ($n = 3-4$). In A and J, P values were obtained from one-way ANOVA with Dunnett’s multiple comparisons test. In D, E, and H, P values were obtained from two-tailed, unpaired Student’s t test. In K, P values were obtained from two-way ANOVA with Sidak’s multiple comparisons test (vs. 24 h within groups). RLU = relative luminescence units.

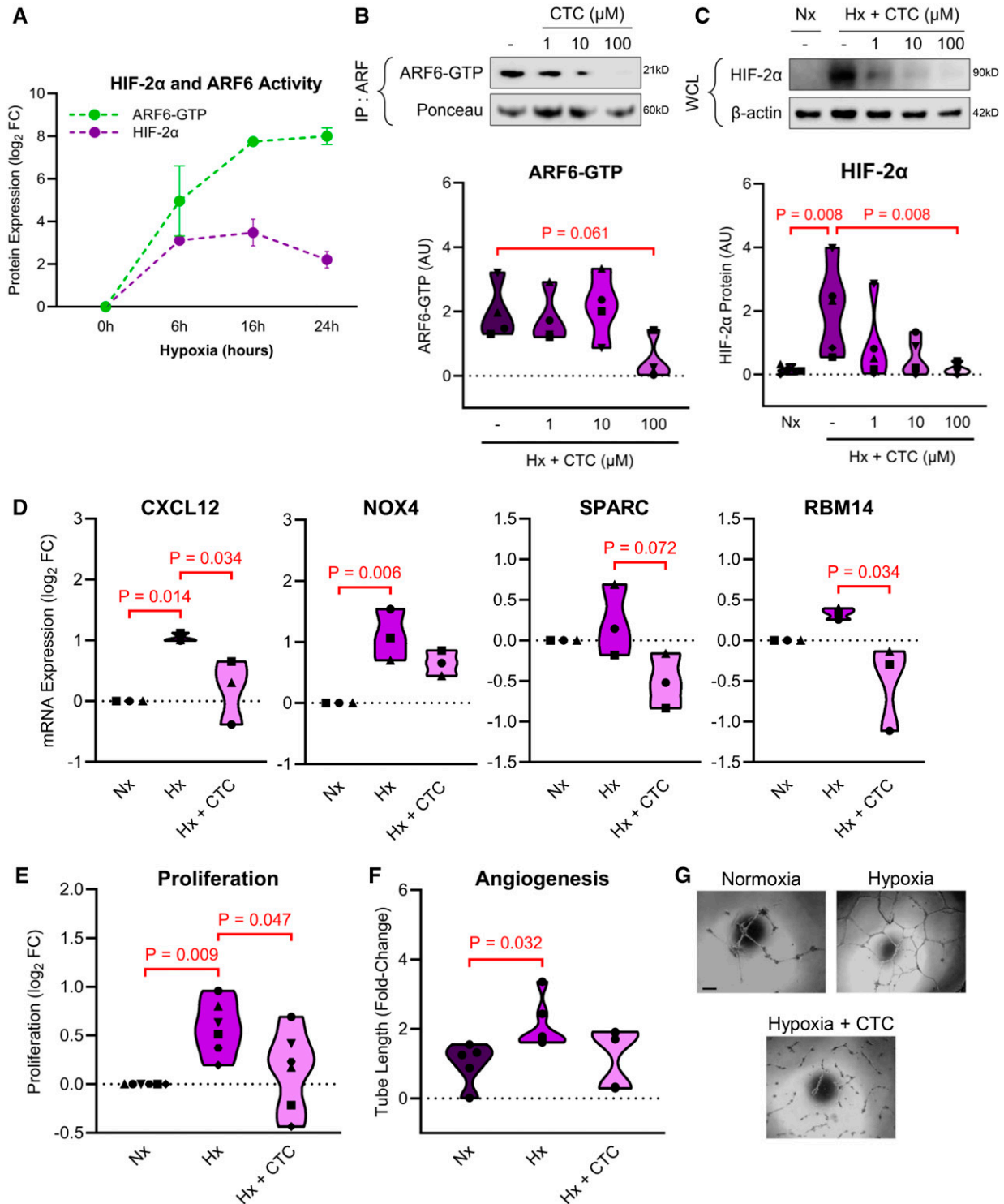


Figure 4. ARF6 inhibitor chlortetracycline (CTC) modulates HIF activation in hypoxia. (A) Quantification of active ARF6-GTP and HIF-2 α during hypoxia (1% O₂) time course ($n = 4$). Representative Western blots and quantification of (B) ARF6-GTP and (C) HIF-2 α after treatment with increasing concentrations of CTC in hypoxia (Hx, 24 h), compared with normoxic control (Nx). (D) Expression of selected HIF target genes; quantitative PCR, fold-change of control ($n = 3-4$). (E) CyQUANT cell proliferation assay ($n = 6$). (F and G) Graph and corresponding representative images of endothelial tube formation. HPAECs were cultured in serum- and growth factor-reduced medium (0.5% FBS) and were treated, as indicated ($n = 5-6$). Except F, P values were obtained from one-way ANOVA with Tukey's multiple comparisons test. In F, P values were obtained from Kruskal-Wallis test with Dunn's multiple comparisons test. Scale bars, 100 μ m.

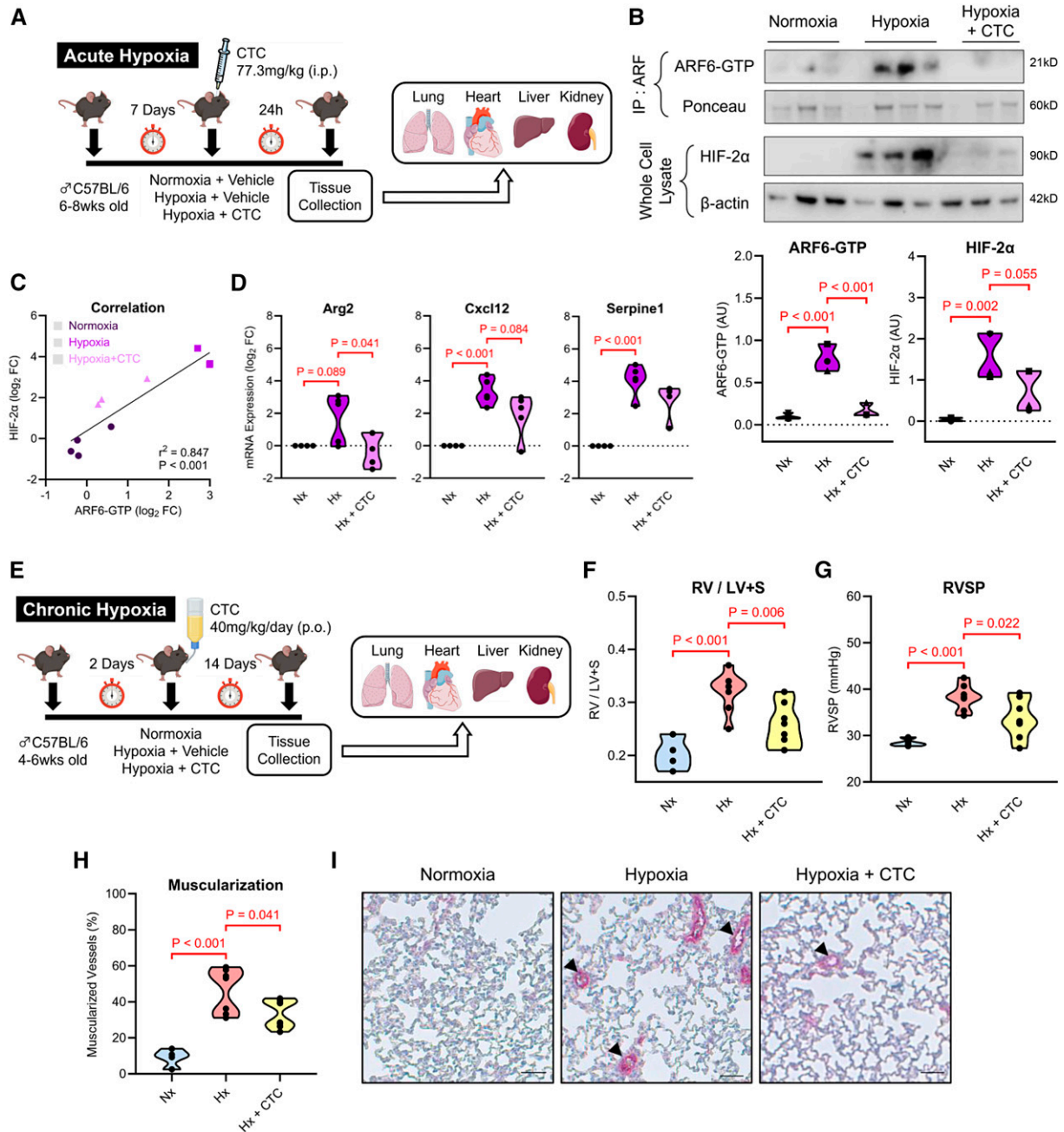


Figure 5. CTC inhibits HIF-2α activation *in vivo* and prevents chronic hypoxia-induced pulmonary hypertension in mice. (A) Experimental outline: CTC (i.p., 77.3 mg/kg) or vehicle (i.p., H₂O) were administered to male (27) control and mice or mice kept in a normobaric hypoxic chamber (10% O₂) for 24 hours, as indicated. Lung, heart, kidney, and liver tissues were collected from all animals. (B) Representative Western blots and quantification of active ARF6 and HIF-2α in mouse lung tissue lysates ($n = 3-4$). (C) Pearson correlation between fold-changes in ARF6-GTP and HIF-2α based on Western blotting analysis; P value was obtained from two-tailed test. (D) Expression of selected HIF target genes by qRT-PCR ($n = 4-5$). P values were obtained from one-way ANOVA with Tukey's multiple comparisons test. (E) Experimental outline: C57BL/6 mice were subjected to Nx or Hx (10% O₂) for 2 weeks. CTC was administered to mice at the onset of hypoxia in drinking water (40 mg/kg/d) (Hx + CTC). (F) Quantification of the RV/LV + S ($n = 4-8$). (G) Quantification of the RVSP in mice after 2 weeks ($n = 4-8$). (H) Quantification of the number of muscularized pulmonary arteries expressed as percentage of α-SMA-positive vessels (28) compared with the total number of vessels with diameter < 25 μm ($n = 4-8$). (I) Representative images of lung sections from different study groups, as indicated. Alkaline phosphatase immunostaining, α-SMA shown in pink. Arrowheads point to remodeled vessels. Scale bars, 40 μm. P values were obtained from one-way ANOVA with Tukey's multiple comparisons test. In all experiments, Nx ($n = 4$), Hx ($n = 8$), and Hx + CTC ($n = 8$). RVSP = right ventricular systolic pressure; RV/LV + S = weight ratio of right ventricle to the left ventricle plus septum.

blood-derived endothelial cells (14), HPAECs (29), and plasma (30) (Figure 6A). ARF6 and PAH shared 24 pathways, including “response to hypoxia,” “endothelin signaling,” “fatty acid metabolism,” “reactive oxygen species production,” “collagen biosynthesis,” and “RNA processing” (Figure 6B), and this association was significant ($P < 0.01$) (Figure 6C). ECFCs are commonly used as accessible surrogates for studying endothelial function in PAH (31). Healthy and PAH ECFCs responded to hypoxia in a similar manner to HPAECs, showing a CTC-responsive activation of ARF6 and HIF-2 (Figures 6D and 6E). No changes to ARF1 activity or HIF-1 α expression were observed (Figures E10A–E10C). PAH ECFCs displayed a markedly enhanced response to hypoxia, manifested by a 4-fold increase in ARF6 activity and a 2.5-fold increase in HIF-2 α expression levels, compared with a 2-fold and 1.5-fold change in respective healthy controls (Figures 6F and 6G). Treatment of PAH cells with CTC reduced ARF6 activity and HIF-2 α expression (Figures 6F and 6G) and affected expression of selected target genes implicated in endothelial dysfunction in PAH, including ING4 (Inhibitor of Growth Protein 4), NOX4 (NADPH oxidase 4), PGK1 (Phosphoglycerate Kinase 1), and RBM14 (RNA binding motif protein 14) (Figure E10D).

Identification of an ARF6-EGFR Interaction by AlphaFold-Multimer

The mechanism of ARF6-induced HIF-2 α activation is likely to be complex, given the high number of upstream regulators and downstream effectors of both proteins (7, 24). Our proteomics data link ARF6 activation with EGFR (epidermal growth factor receptor) activity as well as other pathways, such as PI3K-Akt and Ras-MAPK (Figures 7A and E10A), all implicated in the regulation of HIF (32–37). ARF6 interacts with protein partners via structural elements, which adopt distinct conformations upon binding to GDP and GTP (38) (Figure 7B). To address how activated GTP-bound ARF6 (ARF-GTP) could interact with candidate proteins from our proteomic and bioinformatic analyses, we used AlphaFold-multimer structure prediction (38, 39). A complex between ARF6-GTP and the cytoplasmic domain of EGFR achieved the highest scores (overall predicted score = 0.8; interface predicted score = 0.6), indicating both a correct fold and a likely interface prediction (40) (Figure 7C). More in-depth

predictions suggest that ARF6-GTP interacts with the C-lobe of the EGFR kinase domain via its interswitch and switch loops (Figure 7D), with F47, W62, and Y77 protein-binding residues implicated in the interaction interface (41, 42). The confidence of this interaction is reinforced by low predicted alignment error (Figure 7E). The importance of EGFR in ARF6-mediated HIF activation was validated experimentally using the highly specific EGFR inhibitor gefitinib, which prevented the ARF6-induced accumulation of HIF-2 α protein, with similar efficacy to that seen with MK-2206 and CTC (Figure 7F). In support of a potential role for Akt, we observed a significant CA-ARF6-induced phosphorylation of Akt on S473, necessary for its full activation (43) (Figure E10B). Furthermore, specific inhibition of Akt by MK-2206 (1 μ M) (44) and inhibition of ARF6 by CTC reduced ARF6-induced HIF-2 α expression (Figures 7F and E11C), with no change in expression of total ARF6 (Figure E11D). Importantly, inhibition of EGFR, Akt, and ARF6 all prevented an increase in cell proliferation induced by CA-ARF6 (Figure E11E). Also, CA-ARF6 results in increased phosphorylation of EGFR, a key indicator of activation (Figure E11F). Overall, our data uncover a novel cellular mechanism of HIF activation, involving direct interaction between active ARF6 and EGFR and subsequent upregulation of the PI3K-Akt and Ras-MAPK signaling (Figure 7G).

Discussion

This study is the first to describe ARF6-induced changes in the pulmonary endothelial proteome and reveal a novel link between ARF6 with HIF-2 signaling, important in the pathogenesis of PAH. ARF6 regulates numerous processes of critical importance in PAH, such as endocytotic trafficking, actin polymerization, cell migration, proliferation, angiogenesis, and energy metabolism (5, 8). ARF6 has also been implicated in the regulation of membrane trafficking of BMPRII (bone morphogenetic protein receptor 2), the protein critically involved in vascular remodeling in PAH (4). The contribution of ARF6 is likely to extend beyond the regulation of BMPRII, but mechanisms are not well characterized, as the ARF6 proteome and interactome are largely unknown, and current pharmacological

activators and inhibitors are indirect and therefore nonspecific.

To better understand the mechanism of ARF6 actions, we overexpressed four different ARF6 activity mutants in HPAECs, where ARF6 either remained unaltered (WT), was permanently activated (CA), was inactivated (DN), or showed a spontaneously higher rate of GTP exchange and therefore a higher activity than the WT protein (FC). The inclusion of FC was important, as CA and DN, which block the normal cycle of GTP binding, hydrolysis, and GDP release, may exert similar effects (6, 17). The analysis of the endothelial proteome in cells overexpressing ARF mutants revealed a novel link between ARF6 and HIF signaling and confirmed its associations with endosomal trafficking, angiogenesis, and proliferation pathways. Experimental validation showed that active ARF6 increased expression and activity of HIF-2 in endothelial cells under normoxic and hypoxic conditions, *in vitro* and *in vivo*. This investigation focused on the pulmonary endothelium, because of its key role in the initiation and progression of PAH. Considering that ARF6 is expressed, to a varying degree, in all cells and tissues and has a broad spectrum of effectors, future studies should address the role of ARF6 signaling in other cell types.

Our data implicate EGFR, PI3K-Akt, and Ras-MAPK as mediators of ARF6-induced HIF activation (Figure 7G), consistent with previous reports (32–37). A previous report suggests that N-myristoylated ARF6 recognizes palmitoylated EGFR via lipid-lipid interaction to promote the transport of EGFR to the plasma membrane (45). Our AlphaFold predictions uncovered a new direct mode of protein-protein interaction between ARF6 and EGFR, whereby an interface is formed between the interswitch and switch loops of ARF6 with the C-lobe of the EGFR cytoplasmic kinase domain, that is dependent on its GTP-bound state.

ARF6 and HIF2 have comparable effects on crucial processes involved in the development of PAH. These include activating cell proliferation, migration, and angiogenesis and inhibiting mitochondrial respiration (5, 20–24, 46, 47). As proof of concept and to verify the link between ARF6 and HIF-2 activation *in vivo*, we studied the effects of ARF6 inhibition in a preclinical model of chronic hypoxia-induced pulmonary hypertension. The results showed that ARF6 inhibition by CTC was protective and was accompanied by a reduction in

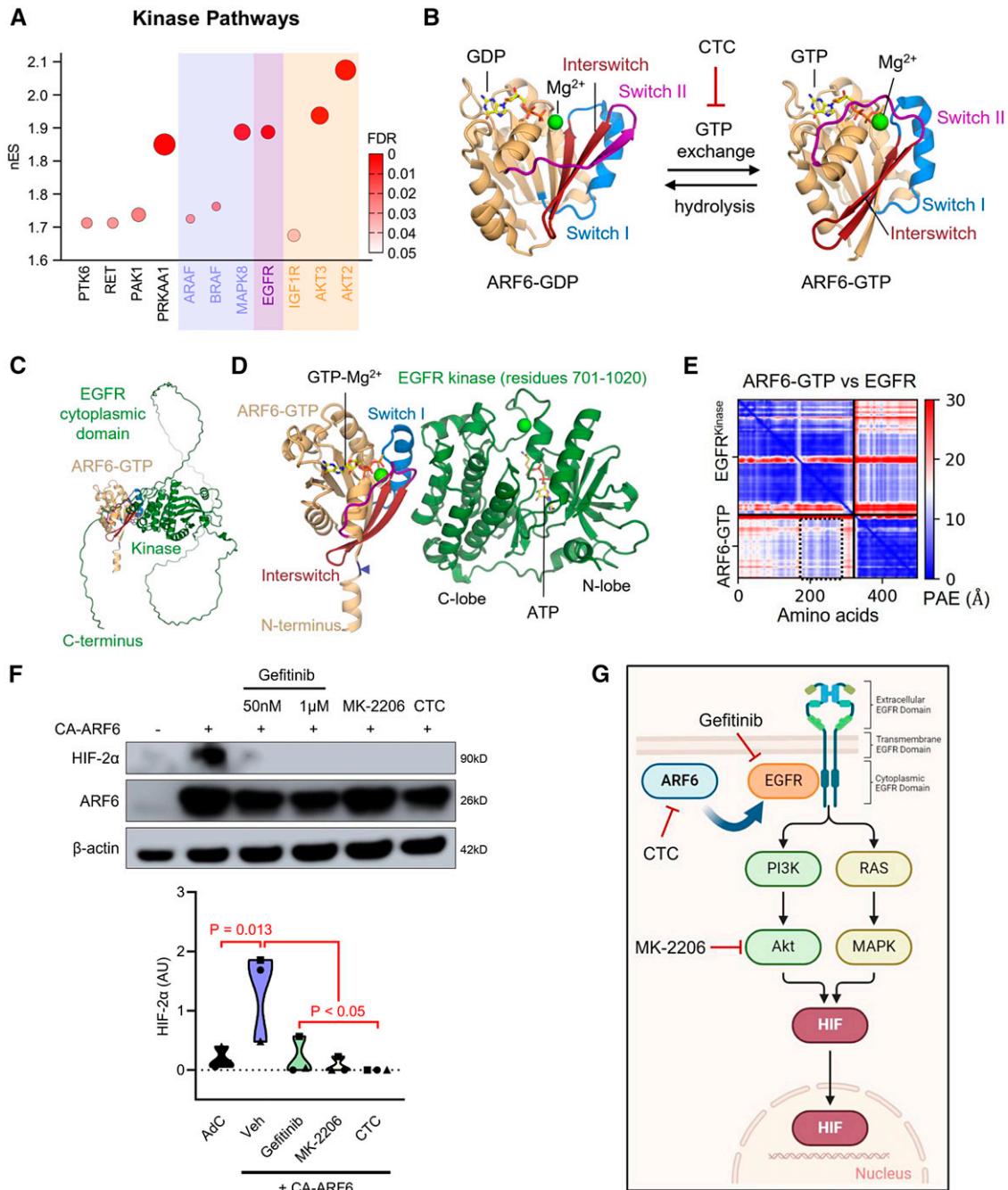


Figure 7. Proposed mechanism of ARF6-mediated HIF activation. (A) Bubble plot showing kinase-related pathways upregulated by CA-ARF6; similar pathways are grouped by colors. (B) Structural basis for GTP cycle of ARF6 (ribbon representation) coupled with conformational changes in structural elements, termed switch I (blue), interswitch (red), and switch II (purple). (C) Structure of an AlphaFold-Multimer prediction of the cytoplasmic domain of EGFR (epidermal growth factor receptor) with activated ARF6 (ARF6-GTP) interacting via the EGFR kinase domain. (D) Structure prediction between EGFR kinase domain and ARF6-GTP. Nucleotide (yellow sticks) and magnesium ions (green spheres) were placed using superposition of the ARF6-GTP crystal structure (PDB 2J5X), and EGFR kinase domain (PDB 2GS6). (E) PAE matrix plots for ARF6-GTP and EGFR. (F) Western blots and corresponding graph showing quantification of HIF-2 α in HPAEC whole-cell lysates after overexpression of CA-ARF6 in the presence of gefitinib at given concentrations (1 μ M in graph) as well as MK-2206 (1 μ M) and chlortetracycline (100 μ M) ($n = 3$). P values were obtained from one-way ANOVA with Dunnett's multiple comparisons test. (G) Schematic of proposed cellular mechanism of ARF6-mediated activation of HIF. PAE = predicted alignment error.

HIF-2 expression in the lung and heart but not in systemic tissues of animals with pulmonary hypertension. This suggests that hypoxia-induced ARF6-HIF signaling may be organ specific. CTC (also known as aureomycin) is a cell-permeant first-generation antibiotic of the tetracycline family, clinically approved for treatment of topical infections and widely used in veterinary medicine. CTC inhibits ARF6 GTP/GDP exchange by interacting with the Mg²⁺ present in the nucleotide binding site of ARF6 and, to a lesser extent, ARF1 (26). As ARF6 activity changes did not

affect ARF1 expression or activity, it is unlikely that ARF1 mediated CTC effects in HPAECs or ECFCs. Unlike other ARF inhibitors, CTC can be administered orally, is quickly absorbed from the gastrointestinal tract, and undergoes minimal metabolic modifications. However, its potential clinical applications may be limited by gastrointestinal adverse effects, and, therefore, more extensive studies will be required to evaluate its suitability as a drug candidate in PAH.

In conclusion, we show that ARF6 is a key mediator in HIF-2 signaling in

pulmonary vascular endothelium. Protective effects of ARF6 inhibition in patient-derived cells and a preclinical model of PAH reinforce the view of ARF6 as a potential therapeutic target in PAH. ■

Author disclosures are available with the text of this article at www.atsjournals.org.

Acknowledgment: The authors thank the staff of the National Institute for Health and Care Research Imperial Clinical Research Facility, Hammersmith Hospital (London, United Kingdom). Figures were created using BioRender.

References

- Schermlay RT, Ghofrani HA, Wilkins MR, Grimminger F. Mechanisms of disease: pulmonary arterial hypertension. *Nat Rev Cardiol* 2011;8:443–455.
- Ranchoux B, Antigny F, Rucker-Martin C, Hautefort A, Pécoux C, Bogaard HJ, et al. Endothelial-to-mesenchymal transition in pulmonary hypertension. *Circulation* 2015;131:1006–1018.
- Tang H, Babicheva A, McDermott KM, Gu Y, Ayon RJ, Song S, et al. Endothelial HIF-2 contributes to severe pulmonary hypertension due to endothelial-to-mesenchymal transition. *Am J Physiol Lung Cell Mol Physiol* 2018;314:256–275.
- Abdul-Salam VB, Russomanno G, Chien-Nien C, Mahomed AS, Yates LA, Wilkins MR, et al. CLIC4/Arf6 pathway: a new lead in BMPRII inhibition in pulmonary hypertension. *Circ Res* 2019;124:52–65.
- Donaldson JG, Jackson CL. ARF family G proteins and their regulators: roles in membrane transport, development and disease. *Nat Rev Mol Cell Biol* 2011;12:362–375.
- Hashimoto S, Onodera Y, Hashimoto A, Tanaka M, Hamaguchi M, Yamada A, et al. Requirement for Arf6 in breast cancer invasive activities. *Proc Natl Acad Sci U S A* 2004;101:6647–6652.
- Grossmann AH, Zhao H, Jenkins N, Zhu W, Richards JR, Yoo JH, et al. The small GTPase ARF6 regulates protein trafficking to control cellular function during development and in disease. *Small GTPases* 2019;10:1–12.
- Gamara J, Davis L, Leong AZ, Pagé N, Rollet-Labelle E, Zhao C, et al. Arf6 regulates energy metabolism in neutrophils. *Free Radic Biol Med* 2021;172:550–561.
- Wojciak-Stothard B, Abdul-Salam VB, Lao KH, Tsang H, Irwin DC, Lisk C, et al. Aberrant chloride intracellular channel 4 expression contributes to endothelial dysfunction in pulmonary arterial hypertension. *Circulation* 2014;129:1770–1780.
- McAlister GC, Nusinow DP, Jedrychowski MP, Wühr M, Huttlin EL, Erickson BK, et al. MultiNotch MS3 enables accurate, sensitive, and multiplexed detection of differential expression across cancer cell line proteomes. *Anal Chem* 2014;86:7150–7158.
- Brenes A, Hukelmann J, Bensaddek D, Lamond AI. Multibatch TMT reveals false positives, batch effects and missing values. *Mol Cell Proteomics* 2019;18:1967–1980.
- Mericó D, Isserlin R, Stueker O, Emili A, Bader GD. Enrichment map: a network-based method for gene-set enrichment visualization and interpretation. *PLoS One* 2010;5:e13984.
- Reimand J, Isserlin R, Voisin V, Kucera M, Tannus-Lopes C, Rostamianfar A, et al. Pathway enrichment analysis and visualization of omics data using g:Profiler, GSEA, Cytoscape and EnrichmentMap. *Nat Protoc* 2019;14:482–517.
- Ainscough AJ, Smith TJ, Haensel M, Rhodes CJ, Fellows A, Whitwell HJ, et al. An organ-on-chip model of pulmonary arterial hypertension identifies a BMPR2-SOX17-prostacyclin signalling axis. *Commun Biol* 2022;5:1192.
- Eva R, Crisp S, Marland JRK, Norman JC, Kanamarlapudi V, Ffrench-Constant C, et al. ARF6 directs axon transport and traffic of integrins and regulates axon growth in adult DRG neurons. *J Neurosci* 2012;32:10352–10364.
- Peters PJ, Hsu VW, Ooi CE, Finazzi D, Teal SB, Oorschot V, et al. Overexpression of wild-type and mutant ARF1 and ARF6: distinct perturbations of nonoverlapping membrane compartments. *J Cell Biol* 1995;128:1003–1017.
- Santy LC. Characterization of a fast cycling ADP-ribosylation factor 6 mutant. *J Biol Chem* 2002;277:40185–40188.
- O'Connell JD, Paulo JA, O'Brien JJ, Gygi SP. Proteome-wide evaluation of two common protein quantification methods. *J Proteome Res* 2018;17:1934–1942.
- Mubeen S, Hoyt CT, Gemünd A, Hofmann-Apitius M, Fröhlich H, Domingo-Fernández D. The impact of pathway database choice on statistical enrichment analysis and predictive modeling. *Front Genet* 2020;11:436.
- Cowburn AS, Crosby A, Macias D, Branco C, Colaço RDDR, Southwood M, et al. HIF2 α -arginase axis is essential for the development of pulmonary hypertension. *Proc Natl Acad Sci U S A* 2016;113:8801–8806.
- Dai Z, Zhu MM, Peng Y, Machireddy N, Evans CE, Machado R, et al. Therapeutic targeting of vascular remodeling and right heart failure in pulmonary arterial hypertension with a HIF-2 α inhibitor. *Am J Respir Crit Care Med* 2018;198:1423–1434.
- Hu CJ, Poth JM, Zhang H, Flockton A, Laux A, Kumar S, et al. Suppression of HIF2 signalling attenuates the initiation of hypoxia-induced pulmonary hypertension. *Eur Respir J* 2019;54:1900378.
- Davis CT, Zhu W, Gibson CC, Bowman-Kirigin JA, Sorensen L, Ling J, et al. ARF6 inhibition stabilizes the vasculature and enhances survival during endotoxemic shock. *J Immunol* 2014;192:6045–6052.
- Semenza GL. Hypoxia-inducible factors: roles in cardiovascular disease progression, prevention, and treatment. *Cardiovasc Res* 2023;119:371–380.
- Bartoszewski R, Moszyńska A, Serocki M, Cabaj A, Polten A, Ochocka R, et al. Primary endothelial-specific regulation of hypoxia-inducible factor (HIF)-1 and HIF-2 and their target gene expression profiles during hypoxia. *FASEB J* 2019;33:7929–7941.
- Macia E, Vazquez-Rojas M, Robiolo A, Fayad R, Abélanet S, Mus-Veteau I, et al. Chlortetracycline, a novel ARF inhibitor that decreases the ARF6-dependent invasive properties of breast cancer cells. *Molecules* 2021;26:969.
- de Jesus Perez V. Making sense of the estrogen paradox in pulmonary arterial hypertension. *Am J Respir Crit Care Med* 2011;184:629–630.
- Ciucan L, Bonneau O, Hussey M, Duggan N, Holmes AM, Good R, et al. A novel murine model of severe pulmonary arterial hypertension. *Am J Respir Crit Care Med* 2011;184:1171–1182.
- Asosingh K, Comhair S, Mavrikis L, Xu W, Horton D, Taylor I, et al. Single-cell transcriptomic profile of human pulmonary artery endothelial cells in health and pulmonary arterial hypertension. *Sci Rep* 2021;11:21086.
- Harbaum L, Rhodes CJ, Wharton J, Lawrie A, Karnes JH, Desai AA, et al.; UK National Institute for Health Research BioResource Rare

- Diseases Consortium, UK Pulmonary Arterial Hypertension Cohort Study Consortium, and US Pulmonary Arterial Hypertension Biobank Consortium. Mining the plasma proteome for insights into the molecular pathology of pulmonary arterial hypertension. *Am J Respir Crit Care Med* 2022;205:1449–1460.
31. Toshner M, Voswinckel R, Southwood M, Al-Lamki R, Howard LSG, Marchesan D, *et al*. Evidence of dysfunction of endothelial progenitors in pulmonary arterial hypertension. *Am J Respir Crit Care Med* 2009; 180:780–787.
 32. Hu ZZ, Du J, Yang L, Zhu YC, Yang Y, Zheng DT, *et al*. GEP100/Arf6 is required for epidermal growth factor-induced ERK/Rac1 signaling and cell migration in human hepatoma HepG2 cells. *PLoS One* 2012;7: e38777.
 33. Giamas G, Hirner H, Shoshiashvili L, Grothey A, Gessert S, Kühl M, *et al*. Phosphorylation of CK1 δ : identification of Ser370 as the major phosphorylation site targeted by PKA *in vitro* and *in vivo*. *Biochem J* 2007;406:389–398.
 34. Gkoutinaku IM, Befani C, Simos G, Liakos P. ERK1/2 phosphorylates HIF-2 α and regulates its activity by controlling its CRM1-dependent nuclear shuttling. *J Cell Sci* 2019;132
 35. Rho JK, Choi YJ, Lee JK, Ryoo BY, Na II, Yang SH, *et al*. Gefitinib circumvents hypoxia-induced drug resistance by the modulation of HIF-1 α . *Oncol Rep* 2009;21:801–807.
 36. Yoo JH, Brady SW, Acosta-Alvarez L, Rogers A, Peng J, Sorensen LK, *et al*. The small GTPase ARF6 activates PI3K in melanoma to induce a prometastatic state. *Cancer Res* 2019;79:2892–2908.
 37. Zhong H, Chiles K, Feldser D, Laughner E, Hanrahan C, Georgescu M-M, *et al*. Modulation of hypoxia-inducible factor 1 expression by the epidermal growth factor/phosphatidylinositol 3-kinase/PTEN/AKT/FRAP pathway in human prostate cancer cells: implications for tumor angiogenesis and therapeutics 1. *Cancer Res* 2000;60: 1541–1545.
 38. Pasqualato S, Ménétrey J, Franco M, Cherfils J. The structural GDP/GTP cycle of human Arf6. *EMBO Rep* 2001;2:234–238.
 39. Jumper J, Evans R, Pritzel A, Green T, Figurnov M, Ronneberger O, *et al*. Highly accurate protein structure prediction with AlphaFold. *Nature* 2021;596:583–589.
 40. O'Reilly FJ, Graziadei A, Forbrig C, Breckenkamp R, Charles K, Lenz S, *et al*. Protein complexes in cells by AI-assisted structural proteomics. *Mol Syst Biol* 2023;19:e11544.
 41. O'Neal CJ, Jobling MG, Holmes RK, Hol WGJ. Structural basis for the activation of cholera toxin by human ARF6-GTP. *Science* 2005;309: 1093–1096.
 42. Ménétrey J, Macia E, Pasqualato S, Franco M, Cherfils J. Structure of Arf6-GDP suggests a basis for guanine nucleotide exchange factors specificity. *Nat Struct Biol* 2000;7:466–469.
 43. Hart JR, Vogt PK. Phosphorylation of AKT: a mutational analysis. *Oncotarget* 2011;2:467–476.
 44. Hirai H, Sootome H, Nakatsuru Y, Miyama K, Taguchi S, Tsujioka K, *et al*. MK-2206, an allosteric akt inhibitor, enhances antitumor efficacy by standard chemotherapeutic agents or molecular targeted drugs *in vitro* and *in vivo*. *Mol Cancer Ther* 2010;9:1956–1967.
 45. Guo H, Wang J, Ren S, Zheng LF, Zhuang YX, Li DL, *et al*. Targeting EGFR-dependent tumors by disrupting an ARF6-mediated sorting system. *Nat Commun* 2022;13:6004.
 46. Liang C, Qin Y, Zhang B, Ji S, Shi S, Xu W, *et al*. ARF6, induced by mutant Kras, promotes proliferation and Warburg effect in pancreatic cancer. *Cancer Lett* 2017;388:303–311.
 47. Befani C, Liakos P. The role of hypoxia-inducible factor-2 alpha in angiogenesis. *J Cell Physiol* 2018;233:9087–9098.